Plasma–surface interactions during tokamak disruptions and rapid shutdowns

E.M. Hollmann [a],[*],[1], G. Arnoux [b], N. Commaux [c], N.W. Eidietis [d], T.E. Evans [d], R.S. Granetz [e], A. Huber [f], D.A. Humphreys [d], V.A. Izzo [a], A.N. James [a], T.C. Jernigan [c], M. Lehnen [f], G. Maddaluno [g], R. Paccagnella [h], P.B. Parks [d], V. Philipps [f], M.L. Reinke [e], D.L. Rudakov [a], F. Saint-Laurent [i], V. Sizyuk [j], E.J. Strait [d], J.C. Wesley [d], C.P.C. Wong [d], J.H. Yu [a]

[a] University of California–San Diego, La Jolla, CA 92093-0417, USA
[b] JET-EFDA, Culham Science Centre, Abingdon OX14 3DB, UK
[c] Oak Ridge National Laboratory, P.O. Box 2008, Oak Ridge, TN 37831, USA
[d] General Atomics, P.O. Box 85608, San Diego, CA 92186-5608, USA
[e] MIT Plasma Science and Fusion Center, Cambridge, MA 02139, USA
[f] Institut fuer Energieforschung-Plasmaphysik, Forschungszentrum Juelich GmbH, D-52425 Juelich, Germany
[g] Associazione EURATOM-ENAE sulla Fusione, Centro Ricerche Frascati, I-00044 Frascati, Rome, Italy
[h] Consorzio RFX, Associazione Euratom-ENAE sulla Fusione, Padova, Italy
[i] CEA, IRFM, F-13108 Saint-Paul-lez-Durance, France
[j] Purdue University, West Lafayette, IN 47907, USA

ARTICLE INFO

Article history:
Available online 20 October 2010

ABSTRACT

Recent progress in understanding of disruptions and in developing methods to avoid disruption damage is presented. Nearly complete mitigation of conducted heat loads has been achieved with high-Z gas jet shutdown. The resulting local radiation heat flash melting in the main chamber might be a concern in ITER, especially with beryllium walls. During the current quench, significant vessel forces can occur due to halo currents I_{halo}; however, these are found to fall reliably below a boundary of (halo current fraction times halo current peaking factor) <0.7 both experimentally and numerically. Numerical simulations indicate that runaway electrons (REs) could cause serious damage to hard-to reach components in ITER, making their suppression a high priority. During the current quench, less than 20% of the density required for collisional suppression of REs appears to have been achieved. Collisional suppression of REs may have been achieved, however, in full-current RE beams with gas injection.

© 2010 Elsevier B.V. All rights reserved.

1. Introduction

Plasma disruptions are a rapid, complete loss of plasma thermal and magnetic energy which can occur in tokamaks due to operation beyond stability limits [1,2]. In future large tokamaks with larger stored energy, the potential for serious wall damage from tokamak disruptions will increase. It is therefore essential that disruptions be taken into account in the design of any future large tokamak such as ITER [3]. Present-day experiments and simulations can help predict the effects of disruptions and help develop methods to mitigate their effects.

The time sequence of a typical disruption is shown in Fig. 1. Often, disruptions are characterized by a precursor such as a growing magneto-hydrodynamic (MHD) mode, as seen in magnetic loops (Fig. 1a). Other types of disruptions are characterized by different precursors; for example, density or radiative limit disruptions are usually characterized by rapidly rising radiated power. Regardless of the initial sequence, all major disruptions exhibit a rapid ($\Delta t \leqslant 1$ ms in DIII-D) thermal quench (TQ) with a complete loss of stored thermal energy (Fig. 1b). This is followed by a slower (of order 10 ms) current quench (CQ) with a complete loss of magnetic energy stored in the toroidal plasma current I_p (Fig. 1c). The decay in I_p gives rise to a toroidal loop voltage and electric field (Fig. 1d) which can accelerate runaway electrons (REs).

Plasma–surface interactions and potential wall damage can occur during each phase of a disruption [1]. During the TQ phase conducted heat loads to the plasma-facing components (PFCs) can result in local melting/sublimation. Typically, TQ conducted heat loads are strongest to divertor strike points; however, conducted TQ heat loads can also occur to main-chamber PFCs. During the CQ, currents can be induced in the conducting vessel walls (eddy currents) or driven by direct contact with the plasma current channel (halo currents). These vessel currents can result in $J \times B$ forces which can damage vessel components. Finally, REs can form during
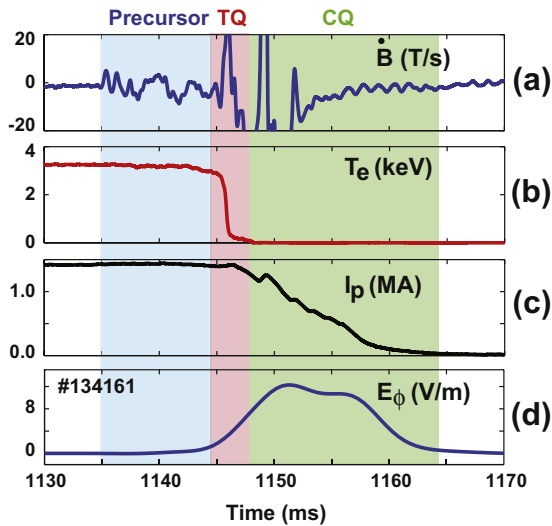
Fig. 1. DIII-D time traces showing common characteristics of a disruption: (a) magnetic fluctuations showing precursor mode and mode slowing/locking; (b) central electron temperature drop; (c) plasma current decay; and (d) increase in toroidal electric field. Shaded bands indicate durations of thermal quench (TQ) and current quench (CQ).

disruptions and rapid shutdowns. These REs can accelerate to high (multi-MeV) energies and very localized damage can result when they strike PFCs.

A variety of methods to mitigate the potentially damaging effects of disruptions are being investigated. Most promising is the injection of a large quantity of impurities into the plasma [4]. The resulting rapid shutdown has a TQ and CQ like a disruption; however, the plasma thermal energy is dominantly radiated (rather than conducted) to the wall, resulting in less localized PFC heating. Also, the resulting CQ plasma tends to be relatively cold and resistive, typically resulting in low halo currents because I_p largely decays before the plasma strikes the wall. A wide variety of rapid impurity injection methods have been used for rapid shutdown of tokamaks: massive gas injection (MGI) [5], small cryogenic pellet injection [6], large shattered cryogenic pellet injection (SPI) [7], shell pellet injection [8], and laser ablation [9]. Routine triggering of MGI to avoid disruption damage has been demonstrated in ASDEX-Upgrade [10].

Methods to avoid forming REs during rapid shutdowns or to suppress REs harmlessly if they do form are also being studied. The deposition of sufficiently large quantities of impurities during the rapid shutdown could, in principle, slow down and thermalize REs via collisional drag [11]. Applied magnetic perturbations could create or expand ergodic magnetic field regions in the plasma, resulting in enhanced RE loss to the wall prior to RE acceleration and avalanche [12]. Magnetic feedback control of RE beams can be used to prevent REs from hitting the wall [13], while reverse loop voltages can be applied to slow down REs [14].

This paper is organized as follows: Section 2 discusses TQ heat loads during disruptions and rapid shutdowns, Section 3 discusses CQ vessel forces during disruptions and rapid shutdowns, and Section 4 discusses disruption REs, their effect on the PFCs, and attempts to mitigate them. Finally, Section 5 contains a brief summary.

2. Thermal quench heat loads

2.1. Disruptions

TQ heat loads are often characterized by a "damage parameter" $\Phi_D \approx [W_{th}/(A_{TQ}\Delta t_{TQ}^{1/2})]$, where W_{th} is the plasma thermal energy,

A_{TQ} the heat deposition area, and Δt_{TQ} the TQ duration. Typical desired operational limits on the damage parameter are e.g. $\Phi_D \approx 15$ MJ/m^2/s$^{1/2}$ for beryllium melting or $\Phi_D \approx 40{-}60$ MJ/m^2/s$^{1/2}$ for tungsten melting or graphite sublimation [2]. Damage parameters estimated for ITER disruptions can be huge, $\Phi_D > 10^3$ MJ/m^2/s$^{1/2}$, clearly motivating the need for mitigation of TQ heat loads. The exact physics setting the TQ duration Δt_{TQ} is not fully understood. In the traditional picture of the TQ, tearing mode island overlap and reconnections create ergodic magnetic field regions with poor thermal confinement [15,16]. A variety of experimental evidence supports this traditional TQ picture. For example, large low-order (poloidal mode number $m = 1$ and 2, and toroidal mode number $n = 1$) perturbations are seen during the TQ with soft X-ray (SXR) and electron cyclotron emission (ECE) diagnostics, consistent with the growth of large tearing modes. During MGI experiments, a delay in TQ onset with varying safety factor q consistent with (2/1) mode onset was observed [17]. Despite this supporting evidence, the TQ duration is not well-matched by basic calculations. Fig. 2 shows measured TQ duration in different tokamaks as a function of minor radius [1]. Simple estimates of the resistive reconnection time and resistive MHD island growth time are also shown; it can be seen that these are of order $10{-}100\times$ too slow to explain the observed TQ duration. Attempts to explain the observed short TQ durations have been made using alternate models such as ballooning fingers [18] or impurity blooms [19]. Still, present estimates of TQ durations in future devices are based on extrapolation.

The physics determining the TQ heat deposition area A_{TQ} is thought to be complex, resulting from a combination of scrape-off layer (SOL) broadening from enhanced TQ cross-field transport, strike point motion and splitting, and sputtered impurity and radiation transport. TQ heat loads have been measured in a variety of tokamaks, usually with IR cameras [20–22]. Examples of IR images in JET during the TQ of two different disruptions are shown in Fig. 3 [23]. Significant heat loads can be seen to strike the lower divertor, upper dump plate, and main chamber limiters. These main-chamber heat loads could have a significant impact on the TQ dynamics, as impurities sputtered from the main chamber can enter the core plasma more quickly and result in fast radiative losses [24]. Calculations of the effective SOL width indicate that the SOL grows during the TQ, typically up to about $5{-}10\times$ larger than the pre-TQ width [23]. Presently, estimates of TQ heat loads in future
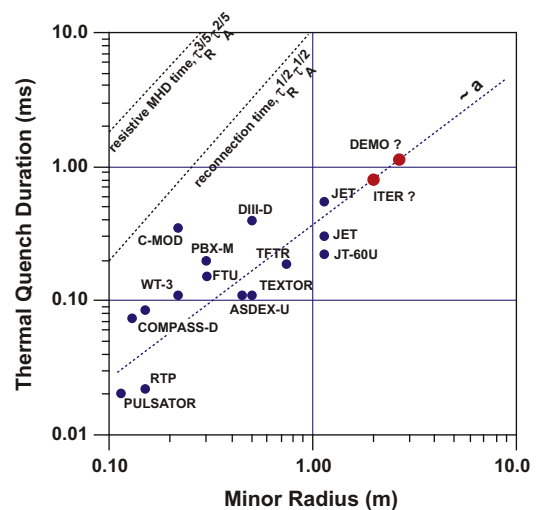
Fig. 2. Measured thermal quench durations as a function of minor radius in different tokamaks (adapted from Ref. [1]). τ_R is the resistive time and τ_A the Alfven time.
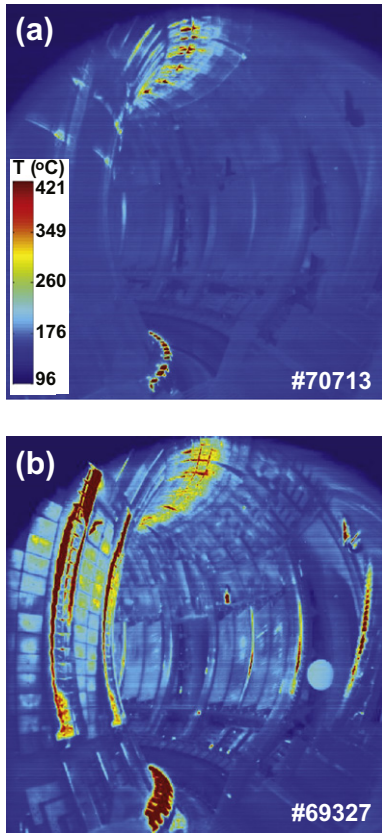
Fig. 3. IR images in JET during TQ of (a) vertical displacement event (VDE) and (b) density limit disruptions (from Ref. [23]).
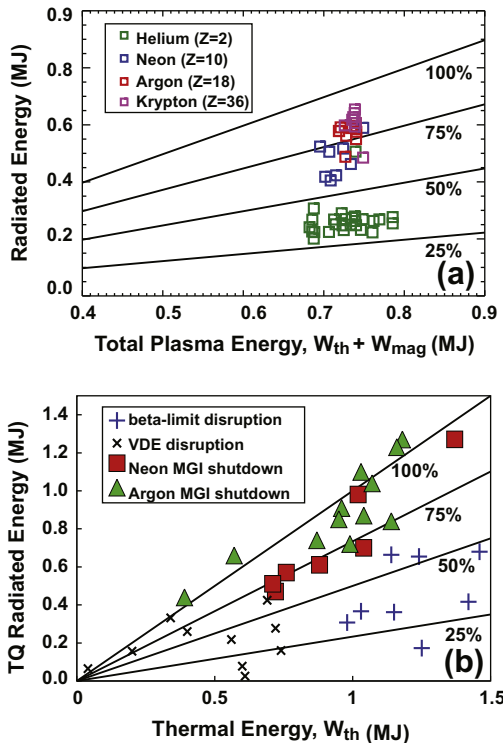

Fig. 4. (a) Total radiated energy as a function of initial plasma thermal + magnetic energy for MGI shutdowns in C-Mod (from Ref. [34]); and (b) TQ radiated energy as a function of initial thermal energy for different types of disruptions and MGI shutdowns in DIII-D (from Ref. [22]).

tokamaks are made by assuming a broadening of order 5–10× in the SOL width during the TQ [25].

In addition to IR imaging such as shown in Fig. 3, TQ-relevant pulsed heat loads have been studied using plasma guns [26], electron beams [27], and simulations [28]. Overall, the main findings are that melt flow tends to dominate the damage to metal surfaces in response to TQ-relevant damage factors: first, a melt puddle is created by the intense heat pulse, and then the metal is mobilized by plasma ∇P or $J \times B$ forces [29,30]. In high-Z metals like tungsten, melt flow is significantly lower than for low-Z metals like Be or Al. It is found that cracking and dust formation tend to dominate the erosion of high-Z metals and carbon composites (CFCs) [29]. Dust formation has been clearly observed in tokamak disruptions using fast camera imaging [31]. Vapor shielding is found to be extremely important, with reductions of 100× or more in localized erosion when vapor shielding is taken into account [32], suggesting that materials can be developed with surfaces which give improved vapor shielding to prevent surface melting. Research is beginning in the area, for example using tungsten mesh infiltrated with low-Z materials [33].

2.2. Rapid shutdowns

Rapid shutdowns have clearly shown the ability to effectively radiate much of the initial plasma thermal energy, thus reducing conducted heat loads. Fig. 4a shows C-Mod massive gas injection (MGI) shutdown data, with total radiated energy plotted as a function of total plasma energy for different species of injected gas [34]. Overall, it can be seen that high-Z injected gases are better at radiating away plasma energy than low-Z gases. Fig. 4b compares MGI shutdowns with disruptions in DIII-D: TQ radiated energy is plotted as a function of initial plasma thermal energy [22]. It can be seen that Ar and Ne MGI can approach the ideal 100% radiated power fraction for total suppression of conducted heat loads, as opposed to disruptions, which typically show <50% radiated power fractions.
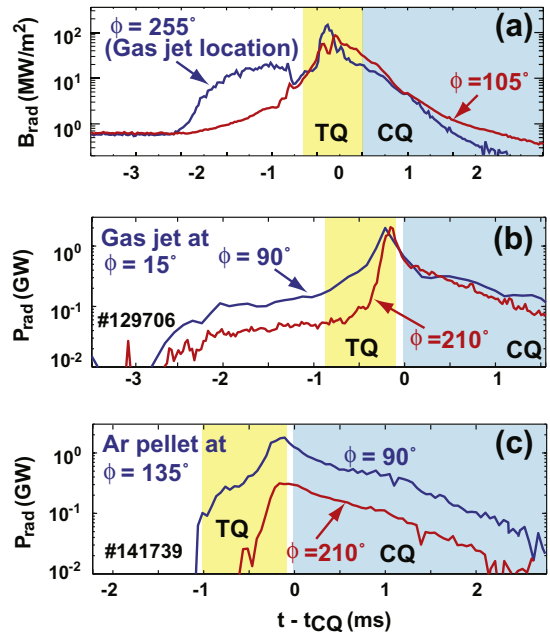

Fig. 5. AXUV fast bolometer measurements of total brightness B_{rad} and/or total radiated power P_{rad} in (a) C-MOD argon MGI shutdown (adapted from Ref. [37]), (b) DIII-D argon MGI shutdown (adapted from Ref. [36]), and (c) DIII-D argon pellet shutdown.

Although rapid shutdowns can achieve near 100% TQ radiation fractions, there is a concern that TQ wall melting could still occur in ITER if the radiated power loads on the first wall are not uniform enough. Calculations indicate that the ITER beryllium first wall will melt with almost any significant non-uniformity in the TQ heat loads [35]. In rapid shutdowns, the radiating impurities are localized to the injection port initially. Subsequent toroidal propagation of MGI injected impurities has been measured with AXUV photodiode arrays and is roughly consistent with sound speed propagation of cold ($T_i \approx 5$ eV) impurity ions [36]. Fig. 5a shows the toroidal propagation of impurities during a MGI shutdown in C-Mod [37]. At the peak of the TQ radiation flash, the brightness is comparable on both sides of the machine. Similar results are seen in DIII-D: Fig. 5b shows total radiated power (calculated under the assumption of toroidal symmetry) measured at opposite sides of the torus during an Ar MGI shutdown [36]. AXUV measurements in small pellet shutdowns indicate that the TQ radiation flash can be less symmetric toroidally, as shown in Fig. 5c; presumably this is because the pellet can penetrate directly into the plasma core and initiate the TQ, thus allowing less time for impurities to move around the torus.

In addition to toroidal transport, the poloidal and radial transport of impurities in MGI shutdowns has been studied. The radial transport of impurity ions appears to be fairly slow ($D_\perp \approx 1$ m^2/s) in DIII-D before the TQ, then extremely rapid during the TQ, and then slower again during the CQ [36]. Poloidal drifts of impurities are shown in Fig. 6 for MGI shutdowns in 6a–c JET [38] and 6e–h DIII-D [36]. There appears to be a tendency for drifts to carry injected impurities over the plasma crown toward the high field side, raising concerns about radiation flash damage to the inboard wall in ITER. The nature and reliability of this poloidal drift has not been studied yet.

Rough estimates for peak wall radiation heat flux arising from MGI shutdowns have been made for DIII-D experiments. This is
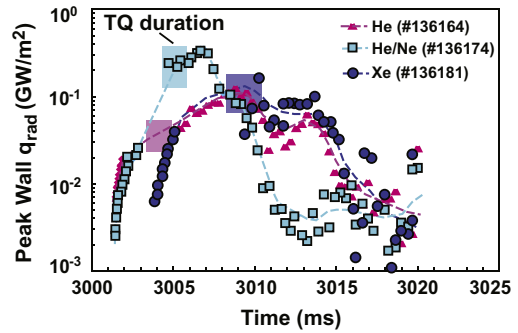

Fig. 7. Peak local wall heat flux as a function of time for DIII-D MGI shutdowns estimated by combining fast camera and fast bolometry data.

done by combining fast camera data with fast bolometer data. Extrapolation between camera and AXUV data is used and analytic estimates ignoring radiation trapping are used to estimate the wall heat flux. Results are shown in Fig. 7 for DIII-D MGI shutdowns. Overall, it can be seen that the peak wall heat flux is expected to occur toward the end of the TQ. It therefore seems reasonable to expect that local MGI port melting in ITER will not be as significant a concern as inboard wall melting. However, further work in this area is warranted before firm conclusions can be drawn.

A possibly beneficial side effect of TQ heat loads is their ability to release hydrogenic atoms stored in the vessel walls. It was suggested previously that intentional rapid shutdowns could be used to lower the tritium inventory in ITER walls [39]. Overall, the amount of H released appears to be of order the initial particle (H) number in the plasma, and is observed to increase with increasing plasma thermal energy. This is shown in Fig. 8a, where D atom release as a function of W_{th} is plotted for JET disruptions [40]. Fig. 8b shows a similar plot for DIII-D disruptions [41]. Two
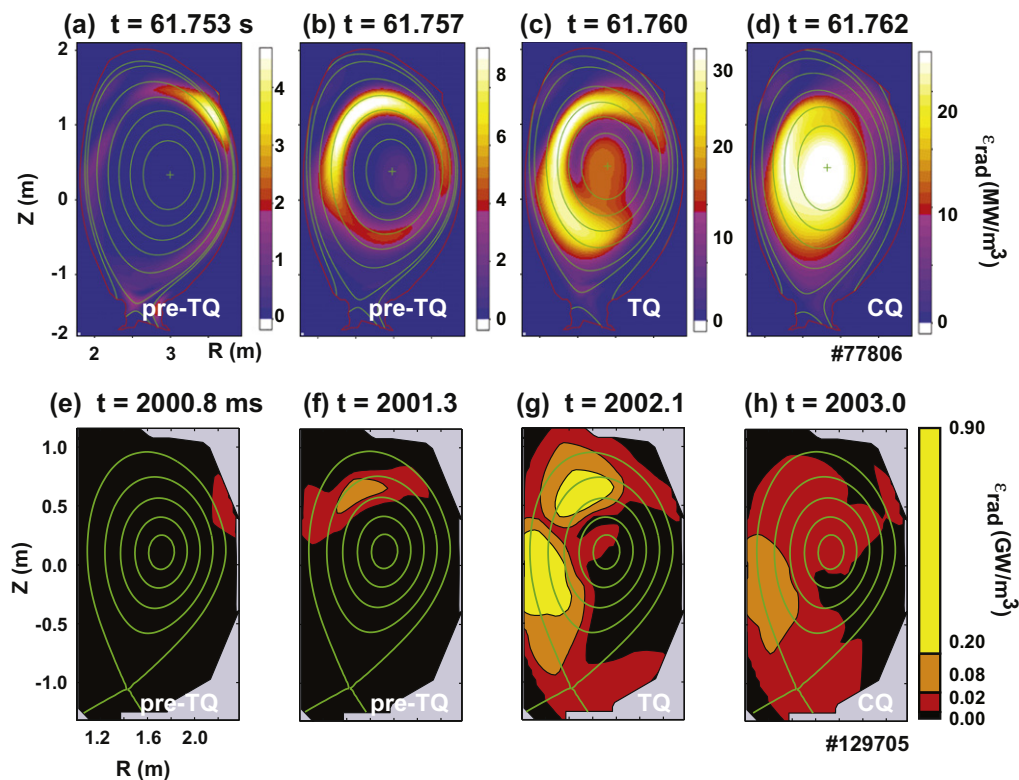

Fig. 6. Fast bolometry of MGI shutdowns at different time steps in (a–d) JET (90% D$_2$/10% Ar MGI) (adapted from Ref. [38]) and (e–h) DIII-D (Ne MGI) (adapted from Ref. [36]).
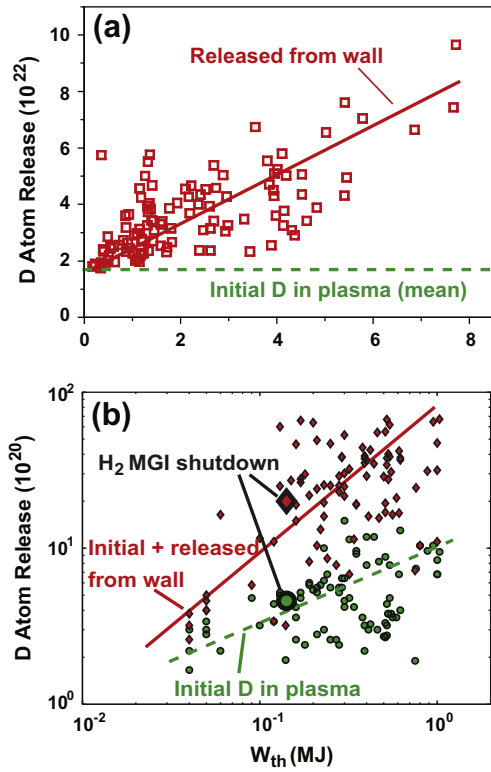
Fig. 8. D atom release from vessel walls by disruptions in (a) JET (adapted from Ref. [40]) and (b) DIII-D (adapted from Ref. [41]) as a function of initial plasma thermal energy.
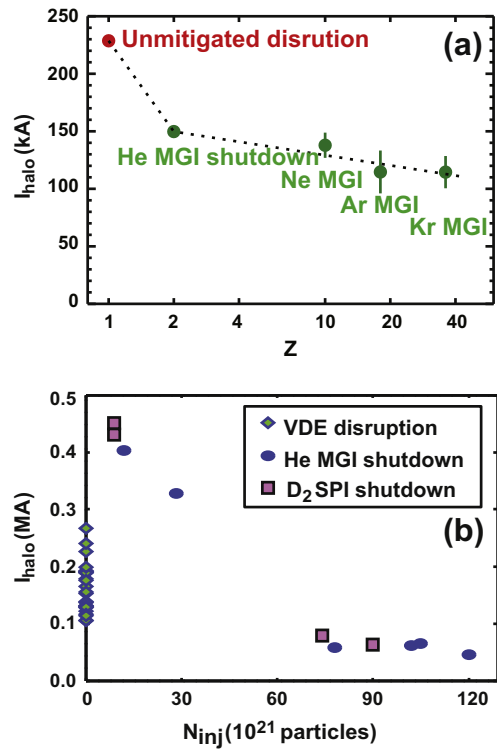

Fig. 10. Poloidal halo currents measured during MGI shutdowns showing (a) I_{halo} vs. Z of gas jet in C-Mod (from Ref. [34]) and (b) I_{halo} vs. number of injected particles (atoms or molecules) N_{inj} in DIII-D for VDE disruptions, He MGI shutdowns, and D_2 shattered pellet (SPI) shutdowns.

during the CQ [42] or due to halo currents which result from direct contact between the plasma current and the wall [1]. Strongest vessel forces are usually observed to occur from halo currents driven by "hot" vertical displacement events (VDEs) where the plasma drifts into the wall before the TQ so that the full plasma current can interact with the conducting wall.

Halo current vessel forces are roughly proportional to poloidal halo current I_{halo} times the toroidal peaking factor $TPF \equiv I_{halo,peak}/I_{halo,ave}$. Present tokamak experiments usually observe $TPF \times (I_{halo}/I_p) < 0.7$ in their disruptions, as shown in Fig. 9. This result has also been achieved in M3D simulations of the ITER CQ, also shown in Fig. 9 [43,44]. Vessel components in future tokamaks can therefore be designed with this limit in mind [45]. Sensitive vessel components can be protected from vessel forces by isolating them from ground [46].

3.2. Rapid shutdowns

Rapid shutdowns are observed to give reduced halo current forces relative to normal disruptions. Higher-Z MGI tends to work better at suppressing halo currents than low-Z MGI, an example of this is shown in Fig. 10a [34]. Weak low-Z rapid shutdown is actually worse than normal disruptions in terms of halo currents—this can be seen in Fig. 10b, where halo currents are plotted as a function of injected quantity N_{inj} for low-Z gas jet and pellet rapid shutdowns. For comparison, halo currents from hot VDEs are shown.

4. Runaway electrons and their wall interactions

4.1. Disruptions

REs can be formed in tokamaks during startup, by RF heating (e.g. lower hybrid or electron cyclotron heating) or during disrup-
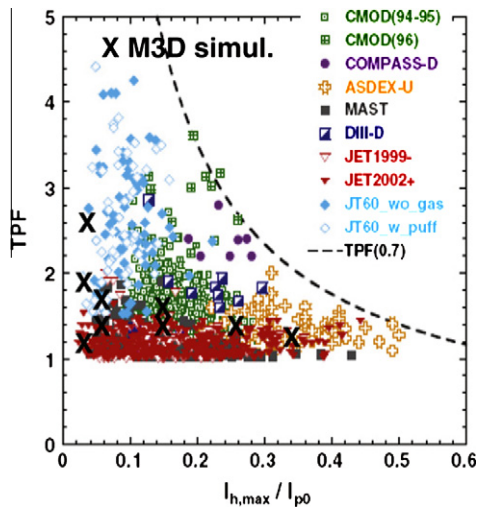

Fig. 9. Disruption halo current data from different machines showing toroidal peaking factor as a function of normalized poloidal halo current. M3D simulations shown also (from Refs. [43,44]).

data points are also shown in Fig. 8b for MGI rapid shutdown, indicating similar results to normal disruptions.

3. Current quench vessel forces

3.1. Disruptions

Current quench vessel forces occur when poloidal currents are driven in conducting vessel components. These currents can result from induced eddy currents due to the decaying plasma current
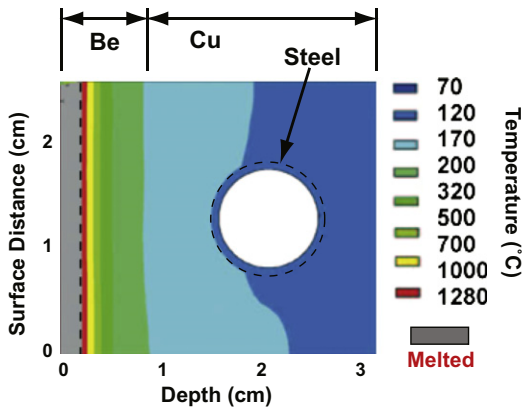
Fig. 11. Simulations of wall armor heating caused by RE-wall strikes in ITER for $\varepsilon = 10$ MeV, $\alpha = 1°$, and $\Delta t = 100$ ms using FLUKA + ANSYS codes (from Ref. [48]).

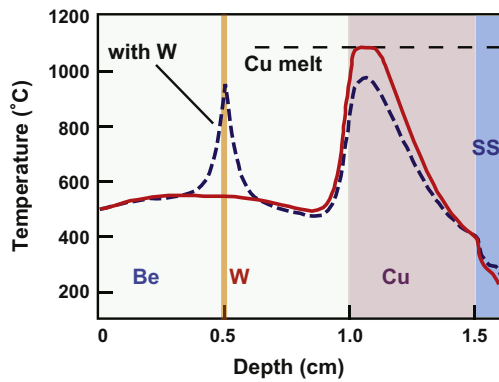**Fig. 12.** Simulations of RE-wall strikes in ITER for $\varepsilon = 50$ MeV, $\alpha = 5°$, and $\Delta t = 10$ ms using HEIGHT code with W layer (dashed curve) and without W layer (solid curve) (adapted from Ref. [49]).

tions/rapid shutdowns. Here, we will focus on REs that form during disruptions and rapid shutdowns. REs have already caused damage to present tokamaks in isolated incidents and are expected to be an even greater concern for larger tokamaks because of the increased predicted CQ RE avalanche gain [47]: $G \approx \exp(I_p/0.5MA) \approx \exp(30)$ in ITER compared with $G \approx \exp(2)$ in present medium-sized tokamaks. This large G in ITER means that even very small initial RE seeds can be converted into large RE currents by the end of the CQ.

Simulations of ITER wall damage resulting from RE-wall strikes have been performed and predict that significant damage can result from even a single full-current RE-wall strike. Fig. 11 shows a simulation using ANSYS plus FLUKA codes of the ITER first wall [48]. The simulation in Fig. 11 assumes RE energy $\varepsilon = 10$ MeV, incidence angle $\alpha = 1°$, and pulse length $\Delta t = 100$ ms, giving a 2 mm thick Be surface melting. Fig. 12 shows, solid curve, a simulated depth profile of temperature resulting from a $\varepsilon = 50$ MeV, incidence angle $\alpha = 5°$, and pulse length $\Delta t = 10$ ms RE-wall strike in ITER resulting in deeper RE penetration [49]. In this case, it was found that the Be surface melting did not occur; instead, melting occurred at the Be–Cu interface. It is possible that a thin layer of tungsten could be used in ITER to absorb some of the RE energy and avoid Be/Cu interface melting [49]; this is shown by the dashed curve in Fig. 12.

It is clearly important to understand as much as possible about disruption REs in order to attempt to avoid or mitigate RE-wall strikes. Presently, many unknowns remain. In theory, RE seed formation is predicted to occur in disruptions via Dreicer evaporation
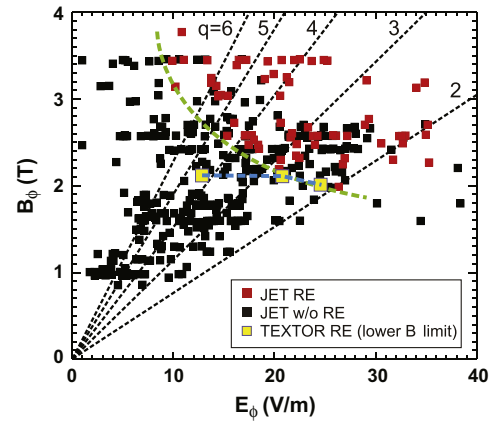

Fig. 13. Shots with RE formation (light squares) and without RE formation (dark squares) in JET suggesting $B_\phi > 2$ T threshold for RE formation (from Ref. [57]).

[50], hot tail formation [51], or reconnection [52]. SXR array contours [53] and IR imaging [54] indicate that REs can form very narrow ($D < 50$ cm) beams. Formation of multiple RE filaments and RE island structure has been observed in startup REs [54,55]. Indirect evidence has been obtained for RE amplification (avalanching) in startup REs [56]. The final disruption RE population is often larger at higher toroidal magnetic fields, with a $B_\phi > 2$ T threshold suggested in various tokamaks [14,57], shown in Fig. 13 for JET. Drag on REs due to whistler wave formation was suggested as a possible source of this trend [58], although this has not been confirmed experimentally. Also, recent experiments on JET have shown that the $B_\phi > 2$ T threshold is not absolute, with trace RE formation observed at lower toroidal magnetic fields $B_\phi = 1.2$ T. Despite these many unknowns, it seems fairly likely that REs will form in ITER disruptions and that steps are necessary to avoid large RE-wall strikes.

4.2. Rapid shutdowns

As in the case of disruptions, many unknowns remain surrounding REs in rapid shutdowns. RE formation can vary considerably from shot-to-shot. Higher-Z species and smaller injected quantities appear to generate more REs [59]. This is shown in Fig. 14, where final (end of CQ) RE current in DIII-D is shown as a function of N_{inj} [8]. Shot-to-shot scatter in RE formation can be seen to be quite large. Also, it is clear that rapid shutdowns are capable of generating significantly more REs than disruptions.

The large scatter in RE formation seen in Fig. 14 is thought to result from variation in the RE seed term and from variation in
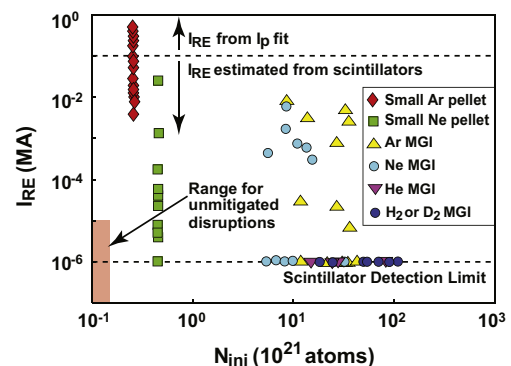

Fig. 14. Final (end of CQ) runaway electron current as a function of number of injected atoms for different types of rapid shutdowns in DIII-D (adapted from Ref. [8]).
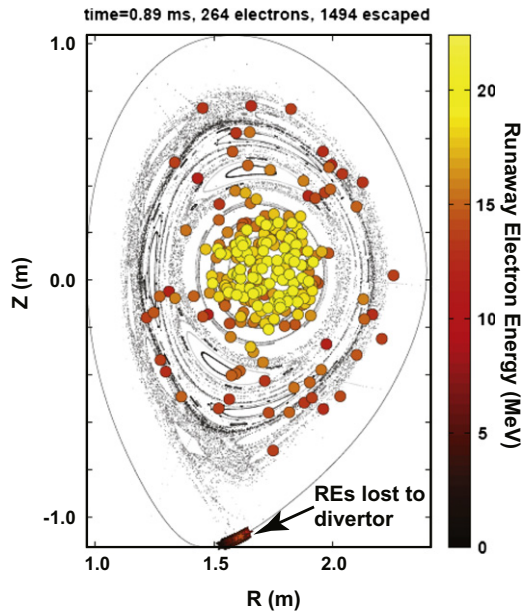
Fig. 15. NIMROD simulations of rapid shutdown in DIII-D showing RE spatial distribution at end of TQ with significant prompt loss fraction into divertor.
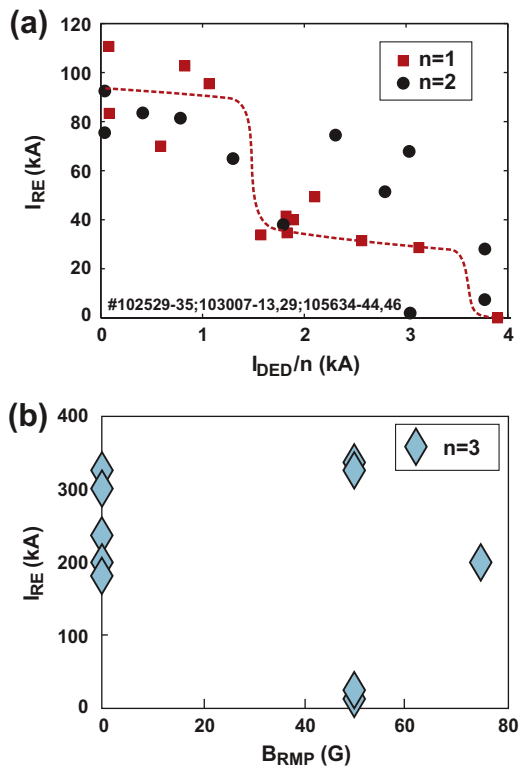

Fig. 16. Final (end of CQ) runaway electron current as a function of applied magnetic perturbation strength for (a) toroidal mode numbers $n = 1$ and $n = 2$ in TEXTOR (from Ref. [61]) and (b) $n = 3$ in DIII-D.

It has been proposed that intentionally applied magnetic perturbations could increase RE prompt loss during rapid shutdowns. Increased RE prompt loss is desirable as compared to late loss REs because (a) these REs have not yet had time to accelerate to high-energy, (b) these REs have not yet avalanched to large currents and (c) the strike location is more predictable (the lower divertor). Preliminary success at using applied fields to enhance prompt RE loss was first indicated at JT-60U [12]. More recently, applied $n = 1$ field perturbations were shown to cause enhanced prompt loss in TEXTOR; results were less clear in the case of $n = 2$ field perturbations, Fig. 16a [61]. Experiments in this area at DIII-D are not conclusive to-date: Fig. 16b shows data from applied $n = 3$ field perturbations where some reduction in final RE current is possible. NIMROD simulations actually predict a decrease in prompt RE loss with applied $n = 1$ or $n = 3$ field perturbations.

Another potential method for reducing final (end of CQ) REs is collisional drag: for sufficiently large total (free + bound) electron number densities $n_{crit} \approx [E_\phi m_e c^2/4\pi e^3 \ln \Lambda]$, collisions are predicted to be frequent enough to drag the REs down in energy [11]. During the ITER CQ, with a predicted $E_\phi \approx 40$ V/m, the required density $n_{crit} \approx 4.2 \times 10^{16}$/cm^3 is quite high [2]. Achieving this density throughout the current channel during the CQ appears to be quite challenging. At present, record line-average, mid-CQ total (free + bound) electron densities appear to be of order $n_{tot} \approx 0.2 n_{crit}$ in DIII-D [8] and possibly even higher in ASDEX-U [8,10], achieved with fast valve MGI, as shown in Fig. 17 for DIII-D MGI shutdowns. One of the main limitations in achieving $n_{tot} \geqslant n_{crit}$ appears to be the finite rise time of the MGI impurity delivery: the early MGI arrivals initiate the TQ and only MGI neutrals which arrive during the TQ are efficiently mixed into the current channel. Injected impurity assimilation efficiencies are found to be of order 20% or less for MGI [36,59]. Firing multiple valves simultaneously appears to be a promising approach for improving n_{tot}: the highest values in Fig. 17 were obtained by firing 5 MGI valves simultaneously.

In future large tokamaks, long gas delivery tubes will probably be required, making the finite rise problem of MGI even worse than in present tokamaks. This suggests the value of investigating alternates to MGI, like shattered pellets (SPI) and shell pellets. The shattered pellet concept fires a large cryogenic pellet against a shatter plate at an angle to create a swarm of ice shards which shut down the plasma. Shell pellets consist of a thin sacrificial shell which burns up in the plasma, exposing a dispersive core consisting of pressurized gas or dust. Promising proof-of-principle experiments on both these methods have been performed recently on DIII-D [8,62].

RE prompt loss at the end of the TQ; as opposed to large variation in the RE late (end of CQ) loss rate or avalanche amplification rate. Large variability in RE prompt loss is consistent with NIMROD simulations [60], such as Fig. 15, which shows that the TQ MHD creates large regions of ergodic field lines, causing REs on larger radii to be lost promptly to the divertor strike points.
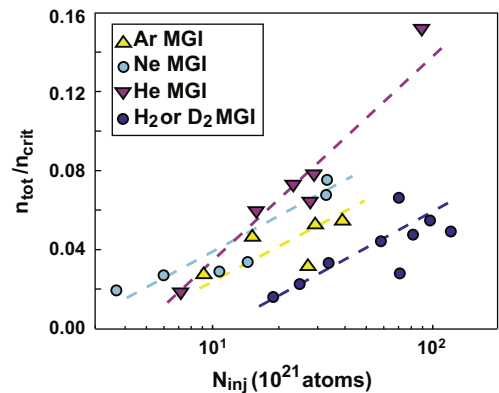

Fig. 17. Line-average mid-CQ total electron density achieved as a function of number of atoms injected for short-pulse MGI shutdowns in DIII-D (adapted from Ref. [8]).

If RE seeds survive the prompt loss phase at the end of the TQ and are sufficiently amplified by the CQ avalanche, they can take over most of the plasma current. Research is underway to come up with methods to avoid a wall strike from a full-current RE beam if one forms. Because conductivity is very high and E_ϕ is low, achieving $n_{tot} \geqslant n_{crit}$ is easier in a full-current RE beam than during the RE seed formation stage. Promising preliminary indications of collisional suppression of full RE beams have been obtained in JT-60U with neon pellet injection [63] and Tore-Supra with MGI [13]. Achieving position control of full-current RE beams is important to allow time for this slow collisional suppression to work. Controlling full RE beams can be challenging because the current channel can be much narrower than what the plasma control system is optimized for. Radial control of a full RE beam has been demonstrated in Tore-Supra [13] and preliminary success at vertical RE beam control has been demonstrated at DIII-D.

5. Summary

Progress has been made in understanding disruptions and developing methods to avoid the damaging effects of disruptions. Because of the potentially severe consequences of even a single unmitigated disruption, because no single mitigation scheme appears ideal for mitigating all forms of wall damage, and because poorly-applied rapid shutdowns can actually worsen wall damage, it is clear that future tokamaks like ITER will need a multi-layer, carefully applied disruption mitigation system. For example, high-Z MGI appears to be the most effective method for mitigating conducted heat loads, but appears to be more likely to generate RE seeds than low-Z MGI. Also, high-Z MGI and high-Z pellets seem to be more likely to cause localized main-chamber wall melting of Be during the TQ radiation flash. Halo currents forces appear to be significantly ($2\times$ or more) reduced by sufficiently massive impurity injection. Halo current forces during unmitigated disruptions appear to be well-bounded by $TPF \times (I_{halo}/I_p) < 0.7$ and can therefore be considered in the vessel wall design of future tokamaks. Simulations indicate that sufficiently high-energy, high-impact angle RE-wall strikes can cause wall melting at inaccessible locations, e.g. Cu–Be braze joints in ITER. A wall strike from a large full-current RE beam at the end of the CQ is probably the single most serious concern for future large tokamaks and research is underway to understand how to mitigate REs at every stage of the rapid shutdown.

Acknowledgments

References

[1] ITER Physics Expert Group on Disruptions, Plasfma Control, and MHD, Nucl. Fusion 39 (1999) 2253.
[2] T.C. Hender, J.C. Wesley, J. Bialek, et al., Nucl. Fusion 47 (2007) S128.
[3] R.J. Hawryluk, D.J. Campbell, G. Janeschitz, et al., Nucl. Fusion 49 (2009) 065012.
[4] S. Putvinski, N. Fujisawa, D. Post, et al., J. Nucl. Mater. 241–243 (1997) 316.
[5] P.L. Taylor et al., Phys. Plasmas 6 (1999) 1872.
[6] G. Pautasso, K. Buchl, J.C. Fuchs, et al., Nucl. Fusion 36 (1996) 1291.
[7] L.R. Baylor, S.K. Combs, C.R. Foust, et al., Nucl. Fusion 49 (2009) 085013.
[8] E.M. Hollmann, N. Commaux, N.W. Eidietis, et al., Phys. Plasmas 17 (2010) 056117.
[9] Z. Yong-Zhen, Q. Ying, Z. Peng, et al., Chin. Phys. B 18 (2009) 5406.
[10] G. Pautasso, D. Coster, T. Eich, et al., Plasma Phys. Control. Fusion 51 (2009) 124056.
[11] M.N. Rosenbluth, S.V. Putvinski, Nucl. Fusion 37 (1997) 1355.
[12] R. Yoshino, S. Tokuda, Nucl. Fusion 40 (2000) 1293.
[13] F. Saint-Laurent, C. Reux, J. Bucalossi, et al., in: Proceedings of the European Physical Society, Division of Plasma Physics (Sofia, 2009).
[14] R. Yoshino, S. Tokuda, Y. Kawano, Nucl. Fusion 39 (1999) 151.
[15] A.B. Rechester, M.N. Rosenbluth, Phys. Rev. Lett. 40 (1978) 38.
[16] A. Bondeson, R.D. Parker, M. Hugon, P. Smeulers, Nucl. Fusion 31 (1991) 1695.
[17] E.M. Hollmann, T.C. Jernigan, E.J. Strait, et al., Phys. Plasmas 14 (2007) 012502.
[18] R.G. Kleva, P.N. Guzdar, Phys. Plasmas 8 (2001) 103.
[19] D.J. Ward, J.A. Wesson, Nucl. Fusion 32 (1992) 1117.
[20] P. Andrew, A. Alonzo, G. Arnoux, et al., J. Nucl. Mater. 363–365 (2007) 1006.
[21] E. Delchambre, G. Counsell, A. Kirk, F. Lott, J. Nucl. Mater. 363–365 (2007) 1409.
[22] E.M. Hollmann, T.C. Jernigan, M. Groth, et al., Nucl. Fusion 45 (2005) 1046.
[23] G. Arnoux, A. Loarte, V. Riccardo, et al., Nucl. Fusion 49 (2009) 085038.
[24] E.M. Hollmann, D.S. Gray, D.G. Whyte, et al., Phys. Plasmas 10 (2003) 2863.
[25] A. Loarte, G. Saibene, R. Sartori, et al., Phys. Scr. T128 (2007) 222.
[26] G. Federici, A. Zhitlukhin, N. Arkhipov, et al., J. Nucl. Mater. 337–339 (2005) 684.
[27] J. Linke et al., J. Nucl. Mater. 212–215 (1994) 1195.
[28] B. Bazylev, H. Wuerz, J. Nucl. Mater. 307 (2002) 69.
[29] H. Wurz, B. Bazylev, I. Landman, et al., J. Nucl. Mater. 307 (2002) 60.
[30] B. Bazylev, G. Janeschitz, I. Landman, et al., J. Nucl. Mater. 386–388 (2009) 919.
[31] D.L. Rudakov, A. Litnovsky, W.P. West, et al., Nucl. Fusion 49 (2009) 085022.
[32] V. Safronov, N. Arkhipov, V. Bakhtin, et al., J. Nucl. Mater. 290–293 (2001) 1052.
[33] C.P.C. Wong, J. Nucl. Mater. 390–391 (2009) 1026.
[34] R.S. Granetz, E.M. Hollmann, D.G. Whyte, et al., Nucl. Fusion 47 (2007) 1086.
[35] D.G. Whyte et al., in: Proceedings of the 22nd Int. Conf. Fusion Energy 2008 (Geneva, Switzerland, 2008) (Vienna: IAEA) IT/P6-18.
[36] E.M. Hollmann, T.C. Jernigan, P.B. Parks, et al., Nucl. Fusion 48 (2008) 115007.
[37] M.L. Reinke, D.G. Whyte, R. Granetz, I.H. Hutchinson, Nucl. Fusion 48 (2008) 125004.
[38] A. Huber et al., these proceedings, 2010.
[39] D.G. Whyte, J.W. David, J. Nucl. Mater. 337–339 (2005) 560.
[40] V. Philipps, M. Freisinger, A. Huber, et al., J. Nucl. Mater. 390–391 (2009) 478.
[41] E.M. Hollmann, N.A. Pablant, D.L. Rudakov, J. Nucl. Mater. 390–391 (2009) 597.
[42] V. Riccardo, P. Barabaschi, M. Sugihara, Plasma Phys. Control. Fusion 47 (2005) 117.
[43] R. Paccagnella, H.R. Strauss, J. Breslau, Nucl. Fusion 49 (2009) 035003.
[44] M. Sugihara et al., in: Proceedings of the 20th Int. Conf. Fusion Energy 2004 (Vilamoura, Portugal, 2004) (Vienna: IAEA) CD-ROM IT/P3-29. <http://www-naweb.iaea.org.napc/physics/fec/fec2004/datasets/index.html>.
[45] M. Sugihara, M. Shimada, H. Fujieda, et al., Nucl. Fusion 47 (2007) 337.
[46] G.F. Counsell, R. Martin, T. Pinfold, et al., Plasma Phys. Control. Fusion 49 (2007) 435.
[47] A.Yu. Sokolov, JETP Lett. 29 (1979) 244.
[48] G. Maddaluno, G. Maruccia, M. Merola, S. Rollet, J. Nucl. Mater. 313–316 (2003) 651.
[49] V. Sizyuk, A. Hassanein, Nucl. Fusion 49 (2009) 095003.
[50] H. Dreicer, Phys. Rev. 117 (1960) 329.
[51] H.M. Smith, E. Verwichte, Phys. Plasmas 15 (2008) 072502.
[52] P.V. Savrukhin, Plasma Phys. Control. Fusion 48 (2006) B201.
[53] R.P. Gill et al., Nucl. Fusion 40 (2000) 163.
[54] I. Entrop, R. Jaspers, L. Cardozo, K.H. Finken, Plasma Phys. Control. Fusion 41 (1999) 377.
[55] R. Jaspers et al., Phys. Rev. Lett. 72 (1994) 4093.
[56] I.M. Pankratov, R. Jaspers, K.H. Finken, et al., Nucl. Fusion 38 (1998) 279.
[57] M. Lehnen, S.S. Abdullaev, G. Arnoux, et al., J. Nucl. Mater. 390–391 (2009) 740.
[58] T. Fulop, H.M. Smith, G. Pokol, Phys. Plasmas 16 (2009) 022502.
[59] S.A. Bozhenkov, M. Lehnen, K.H. Finken, et al., Plasma Phys. Control. Fusion 50 (2008) 105007.
[60] V.A. Izzo, D.G. Whyte, R.S. Grantez, et al., Phys. Plasmas 15 (2008) 056109.
[61] M. Lehnen, S.A. Bozhenkov, S.S. Abdullaev, et al., Phys. Rev. Lett. 100 (2008) 255003.
[62] N. Commaux, L.R. Baylor, T.C. Jernigan, et al., Nucl. Fusion 50 (2010) 112001.
[63] Y. Kawano, N. Tomohide, A. Isayama, et al., J. Plasma Fusion Res. 81 (2005) 593.